Exhaust gases thermal impact simulation on helicopter rear structure using CFD

P. Buet[1], E. Laroche[2], R. Paysant[1], M. Yiao[1]

1 Airbus Helicopters S.A.S., Marseille Provence International Airport, F-13725 Marignane cedex, France, 2 ONERA, Université de Toulouse, 2 avenue Edouard Belin, Toulouse, France

Abstract

Exhaust gases ejected by helicopters engines can be assimilated to jets in crossflow as they interact with a complex flow field composed of rotor downwash, relative wind and ground effect for some flight cases. This jet in crossflow configuration is characterized by a strong temperature gradient between the jet and the crossflow as exhaust gases are ejected at temperatures close to 600°C to 700°C. Their interaction with the external flow field can lead to thermal issues such as the overheating of structural parts or external equipment items and the re-ingestion of hot gases through engine and avionics bays air intakes. Hence, being able to predict exhaust gases trajectory and their turbulent mixing with the surrounding flow is critical for design purpose. The present work investigates the capability of aerothermal CFD simulations to correctly reproduce trajectory and mixing of such flows in order to support design, through two representative configurations. Different Steady RANS and SAS/LES approaches are first compared on a dedicated hot jet in crossflow database collected at ONERA. It is shown that even advanced RANS modelling cannot reproduce the jet mixing with a high level accuracy, contrary to unsteady methods. The suggested unsteady methodology is then applied on a real helicopter wind tunnel experiment and shows a very satisfactory reproduction of the near wall temperature field in the helicopter region of interest.

NOMENCLATURE

VR	velocity ratio, $VR = V_j \ /V_{cf}$
CR	blowing ratio, $CR = \rho_j V_j \ /\rho_{cf} V_{cf}$
D	pipe internal diameter
H	height of the computational domain
T_j	jet static temperature
T_{cf}	crossflow static temperature
ρ_j	jet density
ρ_{cf}	crossflow density
V_j	mean jet velocity
V_{cf}	mean crossflow velocity
Pr_t	turbulent Prandtl number
R	momentum flux ratio, $R = \rho_j V_j^2 / \rho_{cf} V_{cf}^2$
R_{ej}	jet Reynolds number
U	mean flow velocity in the x direction
V	mean flow velocity in the y direction
W	mean flow velocity in the z direction
K	turbulent kinetic energy
ω	specific dissipation rate
ε	turbulent dissipation
ν_t	turbulent (or eddy) viscosity
θ	normalized mean temperature
α_t	turbulent diffusivity
$\overline{u'_i u'_j}$	Reynolds stress tensor
$\overline{u'_i T'}$	Turbulent heat flux vector
HHC	Distance between rotor head and floor
Tcf	Static temperature of the transversal flow
Tj	Static temperature of the jet
MGB	Main Gear Box

1. INTRODUCTION

Exhaust gases ejected by helicopters engines can be assimilated to jets in crossflow as they interact with a complex flow field composed of rotor downwash, relative wind and ground effect for some flight cases. This jet in crossflow configuration is characterized by a strong temperature gradient between the jet and the crossflow as exhaust gases are ejected at temperatures close to 600°C to 700°C. Their interaction with the external flow field can lead to thermal issues such as the overheating of structural parts or external equipment items and the re-ingestion of hot gases through engine and avionics bays air intakes. Hence, being able to predict exhaust gases trajectory and their turbulent mixing with the surrounding flow is critical for design purpose.

Jets in crossflow have been extensively studied and are still at the heart of many research topics. The strong interest for this kind of flow has led to countless publications, as better understanding the corresponding physics is of primary interest for many industrial and natural applications [1][1][2]. Over time, the scope of jets in crossflow applications has grown steadily. First studies were mainly focused on trajectory and dispersion of pollutants of plumes issuing from smokestacks, volcanoes or effluents [4], [5].

Presented at 48th European Rotorcraft Forum, Winterthur, Switzerland, 6. - 8. September 2022

Later on, jets in crossflows have been studied to better understand pitch-up effect caused by lifting jets of Vertical and/or Short Take-Off and Landing (V/STOL) aircrafts during transitional flight phases [6]. This kind of flow is also of primary interest in a gas turbine context as it is involved in film cooling [7], dilution jets and fuel injection. With the increasing use of numerical simulations, many recent studies have been focused on the ability of Computational Fluid Dynamics (CFD) methods to simulate such flows.

Regarding steady state modelling numerous studies have been conducted to investigate the capability of various turbulence modeling approaches to correctly simulate those interaction phenomena. The main conclusion is that standard RANS turbulence models fail to describe the turbulent mixing occurring between the jet and the crossflow [8][9][10][11][12].

Unsteady methods are by essence more adapted to represent the mixing between the jet and the crossflow. One example can be found in Yuan et al [13], who simulated jets in crossflow at velocity ratios VR = V_j/V_{cf} of 2.0 and 3.3 and $Re_{cf} = DV_{cf}/\nu$ = 1050 and 2100 using the LES approach. The obtained profiles for the mean velocity and its associated fluctuations were in good agreement with experimental data. However, the comparison was limited to the centerplane. More recently, Prause et al. (2016) compared various unsteady (including RANS/LES methods) approaches for two jets in crossflow at $R = (\rho_j V^2_j/\rho_{cf} V^2_{cf})^{1/2} = 0.7$ and 1.41 and Rej = DVj/v = 20500 and 82000 respectively. The agreement between tests and LES results was very satisfactory. The hybrid SAS-SST approach provided results which were in good agreement with LES ones in the far field. However, some differences were observed in the injection region due to the transition between RANS and LES modes. On the contrary, URANS-SST did not provide improved results compared to the RANS-SST reference, which suggests the importance of capturing a large part of the turbulence spectrum.

It has to be mentioned that most studies mentioned above were conducted on isothermal flows. In other words, the jet and mainflow share the same temperature. Even when cooling issues are at stake, the temperature difference between the cold and hot sources is usually moderate, rarely exceeding dozens of °K.

Experimental works documenting the behavior of high-temperature jets in cold crossflows are scarce. Kamotani & Greber [14] were among the first to investigate configurations with large temperature difference between jet and crossflow. They studied the influence of jet to crossflow temperature difference, ΔT, for two momentum flux ratios R = 59.6 and 15.3. The authors considered two jet temperatures corresponding to ΔT=24°C and 160°C. At moderate R, they observed that lines of local temperature maxima were similar for both ΔT. However, for higher R, those lines gets closer to the wall as ΔT increases, exhibiting a dependence on jet to crossflow density ratio. A dependence of the flow structure on the temperature difference is confirmed by Harms [15], who reports a greater spreading of the counter-rotating vortices in the case of a hot jet compared to a cold one at the same momentum flux ratio (R = 64).

The question of the interaction of hot gases ejected by the engine with the helicopter structure is therefore a complex one, as the temperature difference can exceed 700°C.

The present work investigates the capability of aerothermal CFD simulations to correctly reproduce trajectory and mixing of such flows in order to support design.

It is built as a two-fold and gradual work. The first part of the study aims at comparing two potential approaches (RANS and hybrid RANS/LES) on a dedicated and well documented experiment. Once the accuracy of those models evaluated on this simple, but representative case, it is then adapted to a realistic mock-up, tested in Airbus Helicopters wind tunnels, which represents the second and more industrial part of the study.

For each test case, the experimental set-up is first described, followed by the modelling and numerical aspects.

2. CHARACTERIZATION AND NUMERICAL MODELLING OF A 400°C HOT JET IN A CROSSFLOW

2.1. Experiment

A detailed experimental database has been generated for two jets in crossflow configurations whose blowing ratio, momentum flux ratio and temperature difference are representative of a helicopter application. The two configurations correspond to a moderately hot (70°C) and a hot (400°C) jet, sharing the same blowing ratio CR=1.54. The experiments were conducted within F2 wind tunnel located at ONERA Fauga-Mauzac Center. The experimental set-up is presented on Figure 1.

Presented at 48th European Rotorcraft Forum, Winterthur, Switzterland, 6-8 September, 2022

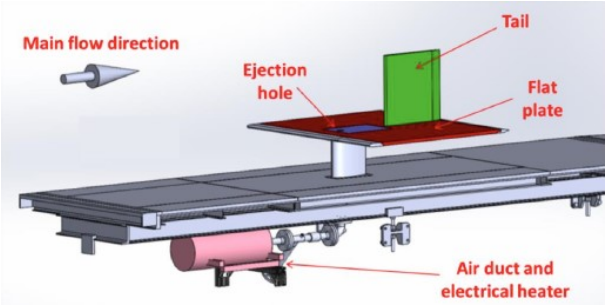

Figure 1 : Vizualisation of the experimental set-up

The jet is produced by a round pipe of internal diameter D=40mm. The pipe is flush-mounted onto a flat plate (red part in Figure 1) with a 90° angle. A fairing is located around the pipe between the flat plate and the wind tunnel floor. This fairing limits flow disturbance due to the presence of the pipe. An insulating material located inside the fairing guarantees the thermal insulation of the pipe. A vertical fin (green part in Figure 1) is located 10D downstream to investigate the interaction of the jet with a part of structure. It was added to represent the interaction of the jet with a helicopter vertical tail fin. The pipe is fed with hot air pressurized at 8 bar and then heated up by two 16kW Leister electrical heaters. The flow leaving the pipe exhibits a fully developed velocity profile in the absence of crossflow. The jet mass flow rate is measured with a Coriolis flowmeter located upstream the heaters. The total temperature of the hot jet is controlled slightly upstream pipe outlet. Jet mass flow and temperature were set to Q_j = 70 g.s^{-1} and T_j = 400°C, leading to a mean jet velocity V_j = 106.2 m.s^{-1} and a jet density ρ_j = 0.52 kg.m^{-3}. Crossflow freestream velocity was set to V_{cf} = 30 m.s^{-1} and its temperature was maintained to T_{cf} = 20°C. A turbulent boundary layer develops on the flat plate upstream jet ejection. Laser Doppler Velocimetry (LDV) measurements were performed 4D upstream jet ejection and show a boundary layer thickness ranging from 3 to 4mm depending on spanwise location. At pipe outlet, the jet exhibits a fully developed velocity profile. Its symmetry has been checked without crossflow. The blowing ratio CR is 1.54, the momentum flux ratio R is 5.45. Particle Image Velocimetry (PIV) and LDV measurements were performed to document the velocity and turbulent fields. In addition, infrared thermography measurements were carried out over the fin surface to characterize the thermal footprint of the jet/crossflow interaction.

2.2. RANS Modelling

2.2.1. Numerical model

Reynolds Averaged Navier-Stokes (RANS) simulations were performed on the configuration presented above with ONERA's finite-volume unstructured compressible code CEDRE. The structured mesh is made of 1.98 million hexahedral elements. The near wall cell size was set to 1 mm leading to y^+=50 except in recirculation areas located upstream and downstream jet ejection. Wall functions were used for all calculations. The wind tunnel and pipe inlets of the computational domain, both placed 4D upstream jet ejection location, are modelled using a mass flux inlet condition. For wind tunnel inlet, an uniform temperature distribution of T_{cf} = 20°C and a mass flux profile were prescribed based on LDV measurements. Mass flux, turbulent quantities and total temperature profiles were specified at pipe inlet using a preliminary RANS calculation of a pipe flow. Pipe inlet conditions were a posteriori checked by comparison between LDV measurements and simulated solution at pipe outlet. A slip condition has been applied to sides and top walls, contrary to the flat plate. All viscous walls are modelled with an adiabatic condition. The outlet is modelled using a pressure condition with a constant value equal to an ambient pressure of 1013.25 hPa. Different classes of turbulence models were evaluated. First of all, first order models were considered. Two isotropic eddy viscosity models (EVM), Dutoya's k-ε and Menter's k-ω SST [8], were selected to evaluate the performance of the industrial standard. The Algebraic Reynolds Stress Model (EARSM) proposed by Hellsten was also considered, being an intermediate with second order models. To address the strong anisotropy present in mixing, two second order models were used, with different dissipation scales: the ω- based Aupoix ATAAC model, and the ε- based EBRSM developed by Manceau. Those models solve additional transport equations for each component of the Reynolds stress tensor.

2.2.2. Flow field results

Profiles of vertical velocity W in the centerplane Y= 0 are presented on Figure 3. Those profiles exhibit two distinct peaks. The first and upper peak, which is present since the beginning of jet development is due to the combination of the vertical component of jet velocity and crossflow deflection by the jet.

Going downstream, a secondary peak located closer to the wall appears. It corresponds to the development of a counter-rotating vortex pair,

Presented at 48th European Rotorcraft Forum, Winterthur, Switzerland, 6-8 September, 2022

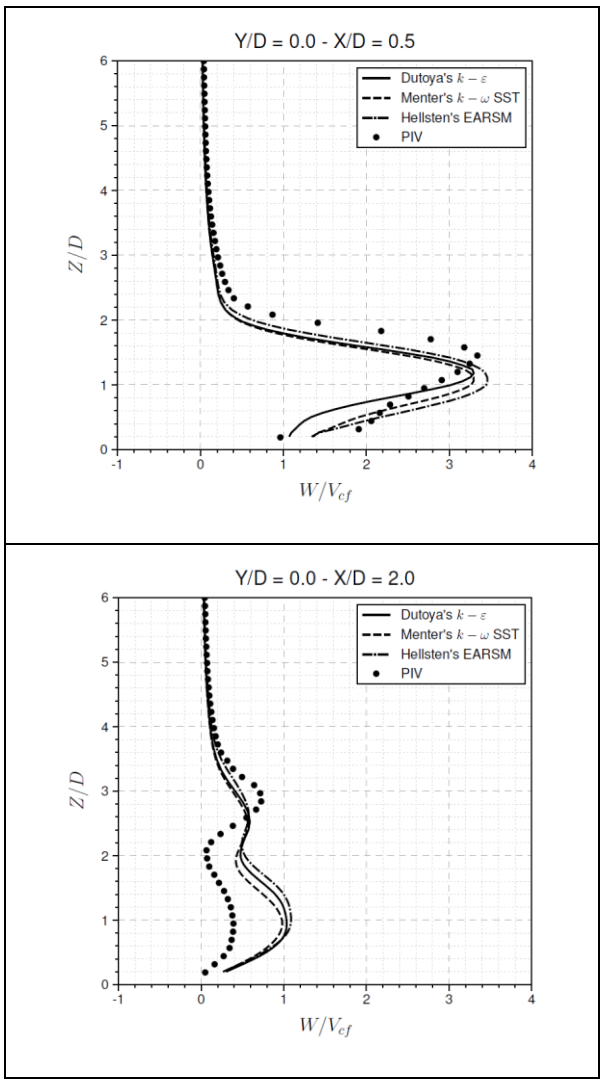

Figure 2 : Profiles of vertical velocity W normalized by crossflow velocity Vcf in the centerplane Y = 0. Simulations performed with first order closure turbulence models

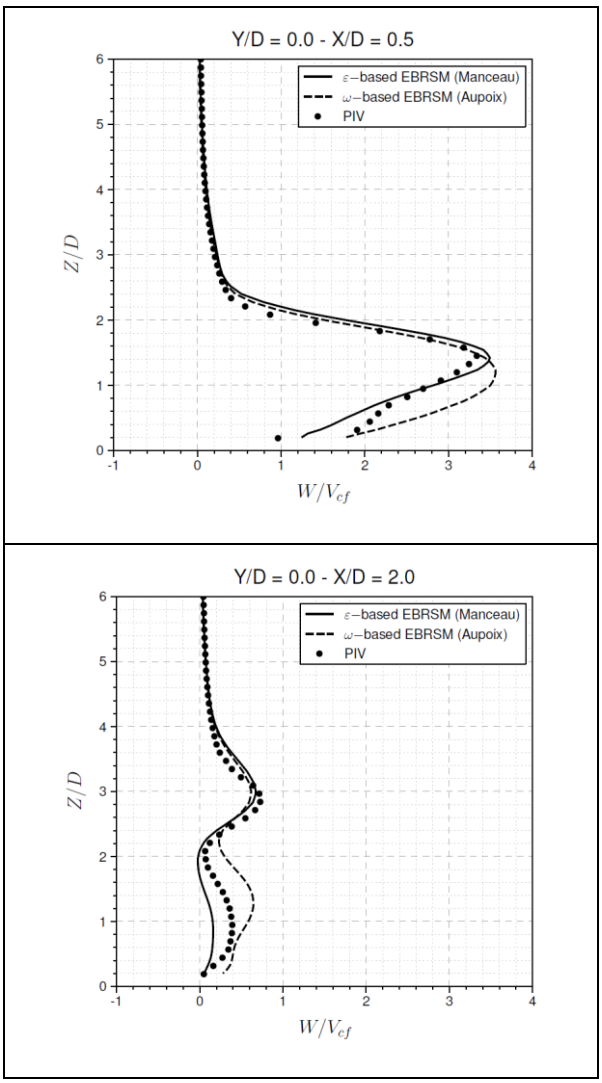

Figure 3 : Profiles of vertical velocity W normalized by crossflow velocity Vcf in the centerplane Y = 0. Simulations performed with second order closure turbulence models

which induces an upward motion in the centerplane. The intensity of the upper peak is fairly well predicted by EVM or EARSM turbulence models at X/D = 0.5, although it is slightly underestimated. On the contrary, its altitude is underestimated, highlighting that jet bending over occurs too early in the simulations. As X/D increases, the intensity of the upper peak diminishes too fast in the simulations. It corresponds to an over-predicted intensity of counter-rotating vortices by all turbulence models. Hellsten's EARSM model [12] which is supposed to better capture turbulence anisotropy does not bring major improvement over models relying on an isotropic eddy viscosity hypothesis. Figure 3 presents the profiles of vertical velocity W in the centerplane Y = 0. The EBRSM model improves the prediction of the upper peak location and intensity compared to first order closure turbulence models. At X/D = 0.5, W profile is therefore reasonably well predicted by the ε-based model while the ω-based one predicts higher velocity levels near the wall. From X/D = 1, the upper peak is only very slightly underestimated and shifted upward. After X/D=2, compared to EVM results, the ε-based EBRSM is in closer agreement with the experiment, while the Aupoix ω-based DRSM exhibits the same trends. Such an analysis reveals the potential of Reynolds Stress Models to better describe the interaction of the jet with the crossflow, but also the major influence of the dissipation scale on the prediction. A more detailed analysis is presented by Paysant [16] and relates the improvement provided by the EBRSM model to a more accurate estimation of the counter-rotating vortices intensity.

Presented at 48th European Rotorcraft Forum, Winterthur, Switzerland, 6-8 September, 2022

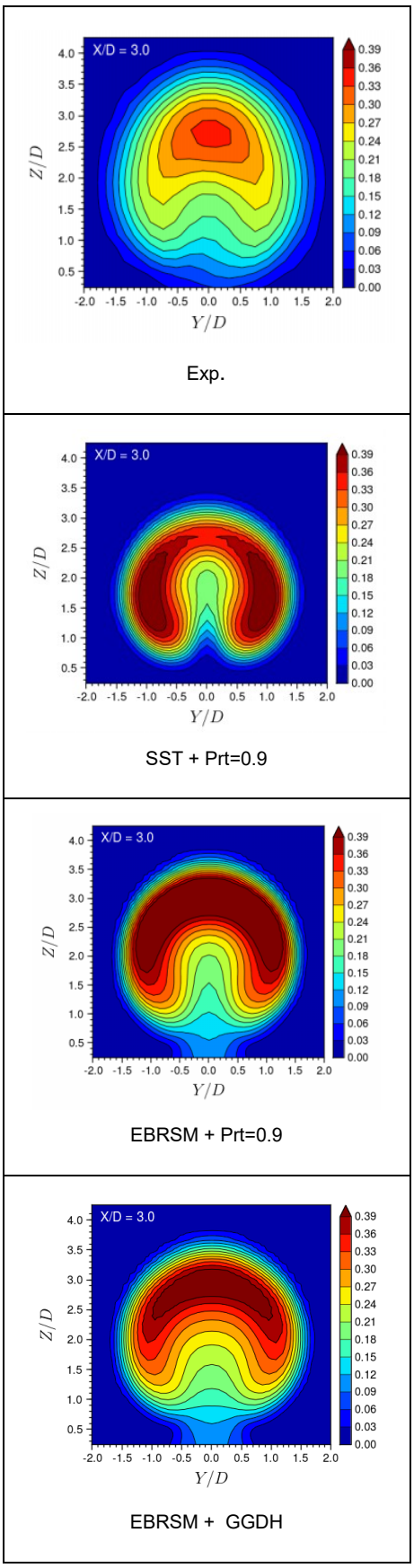

Figure 4 : Comparison of the temperature field between experiment and RANS estimations

2.2.3. Heat transfer results

A systematic comparison to the experimental thermocouple measurements was carried out. Figure 4 presents the temperature field obtained at X/D=3 for the industrial k-ω SST standard, compared to the best RANS estimation, provided by the EBRSM model combined with a Daly Harlow hypothesis for heat transfer (reference as EBRSM + GGDH in the figure). All models tends to underestimate the mixing between the jet and the crossflow, leading to overestimated temperature levels within jet plume. Moreover, for EVM models, two maxima for temperature are located inside the vortex cores. As an example, in the transverse plane located at X/D=3, the maximum temperature is overestimated by +32°C for the k-ω SST. The ε-based EBRSM model provides a better prediction of the thermal field. The temperature maximum remains located inside the jet core, which is in better agreement with experimental findings. However, turbulent mixing is still underestimated by the EBRSM model leading to relatively high temperature levels within jet plume. This underestimation of turbulent mixing is mainly attributed to the fact that the entire turbulent spectrum is modelled in RANS simulations.

2.2.4. Conclusions on RANS modelling

A systematic comparison of various RANS approaches, from the industrial k-ω SST standard to the state of the art EBSRM reveals the large discrepancy between models and detailed measurements. If the velocity is satisfactorily described by the EBRSM, the temperature field is poorly evaluated by all models, due to the crude description of the counter-rotating vortices. This conclusion supports the need for an evaluation of hybrid RANS/LES or LES approaches which are more adapted to describe mixing phenomena dominated by large unsteady structures.

2.3. Scale resolving unsteady simulations

Scale-resolving simulations have been carried out on the high-temperature jet in crossflow configuration investigated during the ONERA F2 wind tunnel. The work being carried out jointly between Airbus Helicopters and ONERA, two Computational Fluid Dynamics (CFD) solvers have been used in the present study. On the one hand, ANSYS Fluent 2019R2 has been defined as the reference software within Airbus Helicopters for aerothermal topics.

Presented at 48th European Rotorcraft Forum, Winterthur, Switzerland, 6. - 8. September 2022

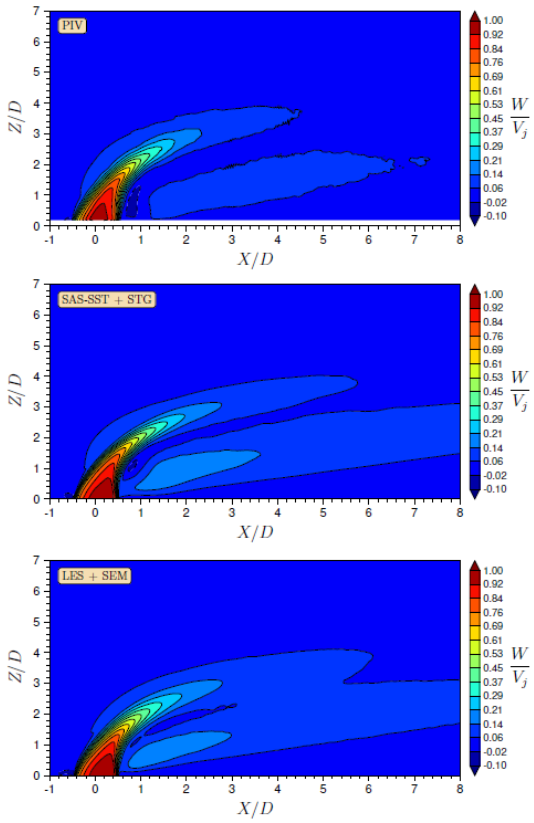

Figure 5 : Mean vertical velocity W field in the centerplane Y=D = 0 normalized by jet velocity Vj . From top to bottom: PIV measurements, SAS-SST+STG and LES+SEM.

On the other hand, ONERA CEDRE has been used as it is the in-house software for multiphysics applications. Both softwares rely on an unstructured finite-volume method to solve Navier-Stokes equations. Moreover, the use of two solvers allowed to compare two potential candidates to simulate the jet in crossflow interaction, namely the Scale Adaptive Simulation technique (SAS) (Ansys Fluent) and the Large Eddy-Simulation approach (CEDRE). Both approaches include synthetic turbulence injection at pipe inlet as results were found to be more accurate in this case. The Synthetic Eddy Model (SEM) method proposed by Jarrin et al.[17] has been used for LES calculations carried out with CEDRE while the Synthetic Turbulence Generator (STG) advocated by Shur et al. [18] relied on SAS-SST calculations performed with ANSYS Fluent. In the rest of the paper, the two approaches will be called SAS-SST+STG and LES+SEM. Details about the meshing strategy and the numerical parameters used can be found in [19], and only the main conclusions are presented here.

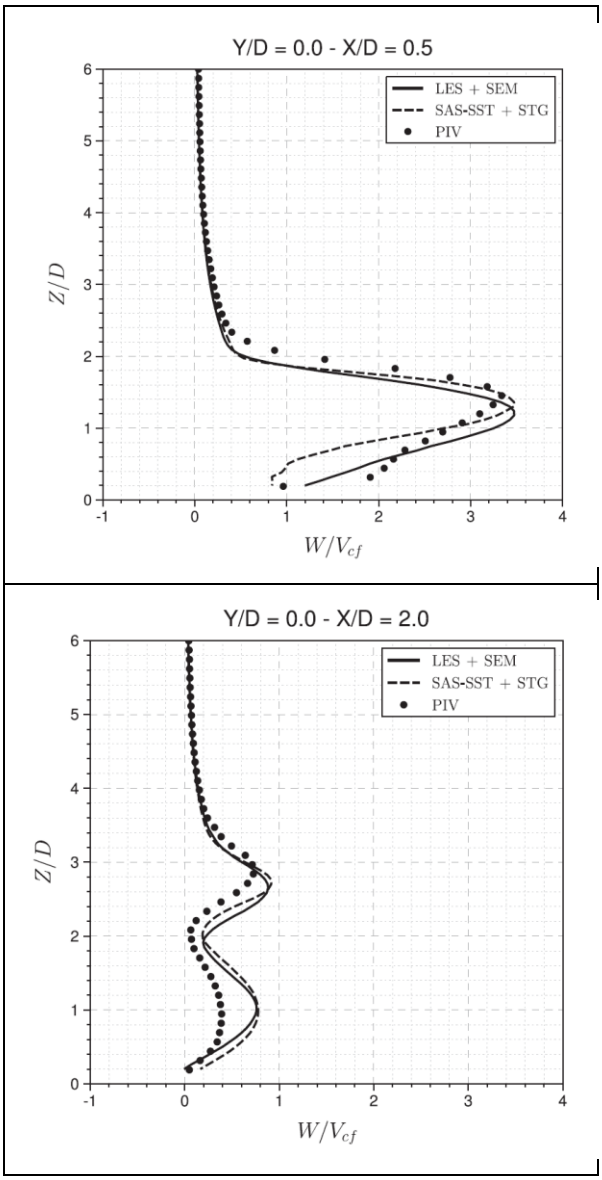

Figure 6 : Time-averaged vertical velocity W profiles in the centerplane Y=D = 0 normalized by crossflow velocity Vcf .

2.3.1. Flow field results

Figure 5 presents the contour plots of the mean vertical velocity W in the centerplane Y/D = 0. It can be seen on the plots that the vertical momentum introduced by the jet is rapidly reoriented. Vertical velocity levels have already dropped down to negligible levels beyond X=D = 4. Below the jet core, a region of upward velocities in the wake is present on the three plots. This upward motion of the flow in the centerplane is induced by the counter-rotating vortices, as mentioned before. Figure 6 represents the mean vertical velocity profiles at X/D=0.5 and X/D=2. The upper peak is correctly captured even though it is located at a

Presented at 48th European Rotorcraft Forum, Winterthur, Switzerland, 6-8 September, 2022

slightly lower altitude compared to the measurements. In contrast, one can notice a premature appearance of the lower peak in simulated profiles. At first, its intensity is largely overestimated with respect to the measurements but as distance downstream increases simulations get in better agreement with the measurements, as X/D=2 profiles indicate. The discrepancies between SAS-SST+STG and LES+SEM techniques are noticeable in the injection region. However, the mean profiles become quite similar for X/D=2.

2.3.2. Heat Transfer results

The temperature field for X/D=3 is compared between experiment and the two unsteady approaches in Figure 7. Contrary to the RANS approaches, the mixing of the jet with the crossflow is correctly captured by the SAS-SST+STG and LES+SEM simulations. The temperature maximum is located in the jet core, on the centerplane. Regarding its vertical location, the LES approach tends to underestimate its altitude at the first two stations (X/D=0.5 and 1.5) but catch-up with measurements at X/D=3.0 (see Figure 7). Reasonable discrepancies between measured and simulated profiles can be observed. A detailed analysis, of the flow and turbulent structures is provided in [19]. This better performance of unsteady methods is connected to the ability of capturing the counter-rotating vortices more precisely than RANS modelling.

2.4. Conclusion on suitable numerical methods for the simulation of a hot jet in an ambient crossflow

The elements provided above, confirm that:

1) Advanced anisotropic models definitely provide an improvement in the hot jet mixing description, compared to classical/industrial EVM

2) However, even this improvement does not bring a satisfactory estimation of the temperature field, due to the rather poor prediction of the counter-rotating vortices intensity

3) Unsteady methods do bring a clear improvement of the temperature field prediction, being able to estimate the large scale mixing.

As a matter of fact, the next paragraph will present an application of the unsteady methodology to a helicopter mock-up, more representative of a realistic configuration.

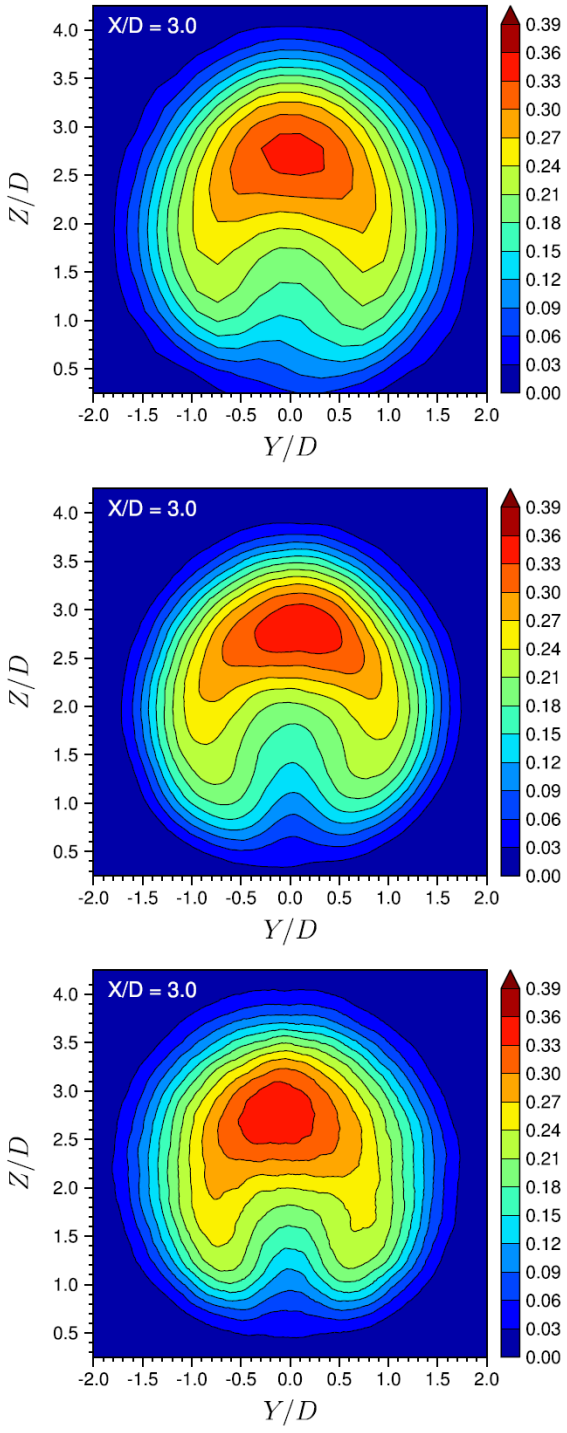

Figure 7 : Normalized mean static temperature fields θ = (T - Tcf)/(Tj - Tcf) in transverse plane (X/D = 3.0). Thermocouples measurements (top), SAS-SST+STG (middle) and LES+SEM (bottom)

Presented at 48th European Rotorcraft Forum, Winterthur, Switzerland, 6-8 September, 2022

3. WIND TUNNEL TESTS

This section describes the wind tunnel tests used to gather experimental data and build up the helicopters experimental database. These tests aim at measuring the temperature increase on the rear fuselage induced by the exhaust gases ejected by the nozzle during different flight cases. This experimental database will be compared to numerical results in the next paragraph.

3.1. Airbus Helicopters wind tunnel

The test campaign was performed in Marignane Airbus Helicopters facility on an EIFFEL-type, open jet wind tunnel. The open jet area is 2.7 meters long and 3 meters diameter. The wind tunnel collector has a contraction ratio of 6.25 and sucks the air from the hall, which is 30.65 meters long and 13.30 meters high. A 10-blades fan with a constant pitch of 5.6 meters diameter generates the airflow, powered by a 350kW direct current electrical engine. The fan speed control allows to tune the airflow velocity in the wind tunnel from 0m/s to 50m/s. The reference [20] provides further technical details about the Marignane Airbus Helicopters wind tunnel.

3.2. Helicopter mock-up and experimental set-up

Figure 8 shows the helicopter mock-up used during the test campaign.

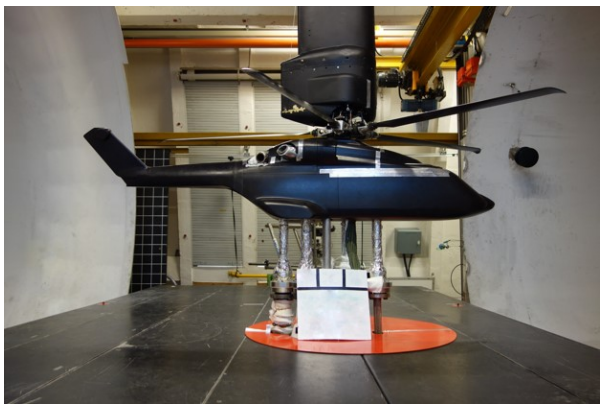

Figure 8 : Helicopter mock-up in the wind tunnel – the air flows from right to left.

The mock-up is fitted with a 5-blades rotor. The rotor twisting law is representative of a serial helicopter. Collective and cyclic controls can be tuned to simulate different attitudes and rotor thrusts. The rotor is not directly attached to the helicopter mock-up due to the size of the rotor engine. Therefore the rotor engine is attached on the upper wall of the wind tunnel, above the helicopter mock-up, and is linked to the rotor hub through a transmission shaft. The transmission shaft is enclosed in a streamlined fairing (black fairing shown on Figure 8) in order to minimize the impact on the wind tunnel airflow. During the tests, the distance between the floor and the rotor head H_{HC} is set to half the rotor's diameter D_R, which is representative of in-ground effect flight cases. The orange zone shown on Figure 8 can be rotated in order to simulate different wind headings.

As shown on Figure 9, the mock-up is fitted with:

- three pipes representing the nozzle exhausts (red),
- one pipe representing the main gear box compartment exhaust (yellow),
- two pipes representing the engine compartment ventilation air intakes (in cyan).

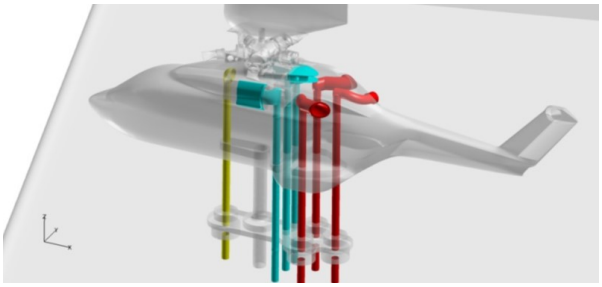

Figure 9 : Hot gaz ejection system (red and yellow) and suction system pipe (cyan)

The flow characteristics (mass flow rate, temperature) of each pipe system can be tuned. Propane burners are used to heat nozzle exhaust gas to the targeted temperature (T_j/T_{cf} = 21.0). An electrical heater is used for the main gear box exhaust pipe. Temperatures and mass flow rates are measured all along the tests. In order to minimize the thermal impact of the pipes on the mock-up, the pipe system is insulated with several layers of Promat material and the pipes are wrapped all along with Refratex blanket material covered with an aluminum sheet.

The external fuselage of the mock-up is covered with a glass-fiber layer and painted with "MONOPOL black" paint, which allows describing the hot gases impingement on the structure by infrared camera imaging.

4. CONTROL OF TEST CONDITIONS

The test conditions are defined by the blowing and suction rates, the ejection temperatures, the rotor thrust and the velocity of the wind tunnel airflow. All these parameters were set in such a way as to respect the conditions of similarity between the mock-up and a reel helicopter.

Presented at 48th European Rotorcraft Forum, Winterthur, Switzerland, 6-8 September, 2022

Wind tunnel flow

The air velocity inside the wind tunnel is measured through the use of two techniques:

- A Pitot probe,
- A Gill WindSonic ultrasonic anemometer.

The Pitot probe is the standard means for measuring the air velocity inside the wind tunnel. However, it is not very accurate for speeds below 10 m/s due to the pressure sensor used and the Pitot measuring principle in itself. Due to the low low velocities of these tests (between 5 m/s and 15 m/s) the ultrasonic anemometer has been used. Measurement uncertainties are estimated at +/- 0.69 m/s for the Pitot probe and +/- 0.25 m/s for ultrasonic anemometer (wind tunnel facilities evaluation). Finally, note that since the wind tunnel is free-flowing, static pressure and temperature conditions are equal to the external condition ones.

Blowing conditions

The three nozzle blowing circuits are identical. From upstream to downstream, these circuits consist of:

- A propane tank and an air tank both at a pressure of 6 bars,

- Two pressure control valves for air supply (2 bars) and propane supply (1.0 - 1.4 bar),

- A venturi tube to measure the air mass flow and a KHRONE flowmeter H250 to measure propane mass flow,

- An assembly to control the flow of air and gas,

- A combustion chamber,

- An inconel flexible tube insulated with Refratex to transport hot gases to the corresponding ejection system of the mock-up.

To ensure that the air-propane mixture is stoichiometric, valves are used to maintain the same air-to-propane ratio regardless of ejection mass flow rate. Considering the lowest ejection temperatures at the outlet MGB, the air is heated using two electric heaters Leister LHS61L. The air mass flow is generated by a Leister Airpack fan. The relative uncertainty of measurement on mass flows is estimated at approximately 3% (wind tunnel facilities evaluation).

Rotor parameters

Concerning the rotor parameters, the torque produced by the electric motor is measured and controlled during each rotation.

Four thermocouples are also installed at the bearings to measure temperature variations during rotations. A 6-axis balance is used to measure rotor moments and forces. Finally, three displacement measurements, each associated with a rotor head servomotor, are made in order to calculate the attitude of the rotor. The uncertainties of measurements on rotor moments and forces are presented in the Table 1 (wind tunnel facilities evaluation).

F_X (N)	F_Y (N)	F_Z (N)	M_X (N.m)	M_Y (N.m)	M_Z (N.m)
±0.93	±1.24	±2.03	±0.41	±1.02	±0.12

Table 1: Estimation of measurement uncertainties on rotor moments and forces.

5. TEMPERATURES MEASUREMENT CLOSE TO THE FUSELAGE

Temperature levels close to the fuselage are measured using 40 thermocouples installed on the mock-up. A visualization of the location of those thermocouples on the right side of the helicopter mock-up fuselage is shown in Figure 10. They are located at the rear of the fuselage, on the tailboom and are equally distributed between the right and left sides of the mock-up.

These thermocouples are positioned a few millimeters away from the wall in order to avoid the effects of thermal conduction. They measure an air temperature close to the wall. For this reason, they will then be labelled by the acronym "TA_STR" for STRucture Air Temperature.

In addition to these 40 thermocouples, four thermocouples are placed in the fuselage to measure skin temperature. For this reason, they will later be labelled as "TP_STR" for STRucture Wall Temperature.

Figure 10: Visualization of the location of thermocouples on the right side of the fuselage of the helicopter mock-up.

Presented at 48th European Rotorcraft Forum, Winterthur, Switzerland, 6-8 September, 2022

The test procedure consists in measuring, continuously and for a complete rotation of the model, temperature levels at the locations of each thermocouple while hot gases are ejected by the nozzles. The speed of rotation of themock-up is prescribed at 1°/s to minimize the duration of a test point. It should be noted that several rotational speeds have been tested (of 0.3°/s 1°/s) and that measurements for a stabilized heading (1 min) were also carried out. The results were similar and the few observed differences typically exhibit the same measurement dispersion as the one observed between two identical tests. In order to identify flight cases with a recirculation phenomenon (hot gas from nozzle through air intakes engine), thermocouples are placed at the air intakes to detect any temperature increase. Finally, the measurement uncertainty of thermocouples is estimated at about +/-1,5°C (wind tunnel facilities evaluation).

6. TEST CASE NUMERICAL SIMULATION

This part presents the numerical simulation made on a wind tunnel test case. The objective is to verify the ability of the SAS-SST approach to predict the flowpath and mixing of the jet in an industrial application. The choice of the SAS-SST approach is justified by the good restitution of the flow dynamics turbulent mixture for the simplified flow pattern studied previously. Since only temperature measurements have been carried out during these tests, we will focus here only on the hot gases thermal impact on the helicopter structure.

6.1. Wind tunnel test case description

For the selected test point, the mock-up is oriented perpendicular to the axis of the test vein.

The wind tunnel flow comes from the right of the helicopter (pilot direction) simulating a flight case in ground effect with a wind heading = 90°. The angle corresponds to the angle between the axis of the fuselage and the relative wind direction. Its value is between -180° and +180°. It is positive when the relative wind comes from the right of the helicopter (pilot direction) and negative when it comes from the left. For wind tunnel test conditions, an air speed of 9 m/s is measured by the anemometer at the entrance of the test section. Note that this air speed is measured with the helicopter mock-up inside and rotor turning. Since the wind tunnel is free-flowing, the static pressure and temperature inside the test vein are equal to the external conditions.

The rotor rotational speed is 1600 rpm and imposes a thrust of FZ = 72 daN. For blowing conditions, only the circular nozzle on the right side of the helicopter near the tail boom (see Figure 10) is active for the test point considered. All suction systems are also turned off. This avoids potential interactions between different blowing and suction systems that may influence the behaviour of the jet nozzle. Regarding the ejection conditions, the jet nozzle is ejected with a static temperature ratio Tj/Tcf = 21.0. After ejection, the jet is driven back by the rotor downwash and the wind tunnel flow leading to jet in crossflow. In order to calculate the blowing and flow ratios (respectively CR and R) motion quantity of the jet, it is necessary to know the velocity of the transverse flow (combination of rotor blast and wind tunnel flow) close to the nozzle. Not having air speed measurements at this location, an estimation of the air speed is obtained from the simulation. Considering the standard of the vector close to the nozzle, it is possible to obtain a local value of Vcf to calculate the main nozzle ejection characteristics. These are summarized in Table 2.

C_R	R	T_j/T_{cf}	ρ_j/ρ_{cf}	Re_j
1.2	2.2	21.0	0.32	15 300

Table 2: Principales caractéristiques du jet tuyère de la configuration hélicoptère.

6.2. Computational domain & Boundary conditions

The computational domain used for the helicopter simulation includes the entire wind tunnel. This choice is based on Airbus Helicopters' experience and best practices in simulating this kind of configuration. In fact, previous studies have shown that the wind tunnel walls are not far enough from the test area to completely neglect containment effects. However, it is assumed that these containment effects are not of first order in the present study. An overview of the computational domain used for the helicopter simulation is shown in Figure 11.

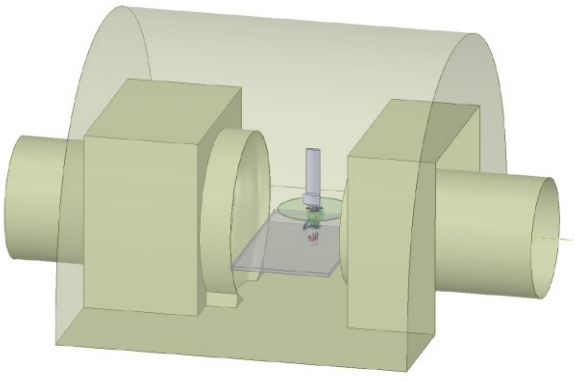

Figure 11 : Visualization of the computational domain used for the helicopter simulation.

Presented at 48th European Rotorcraft Forum, Winterthur, Switzterland, 6-8 September, 2022

A detailed view of the simulated helicopter geometry is shown in Figure 12.

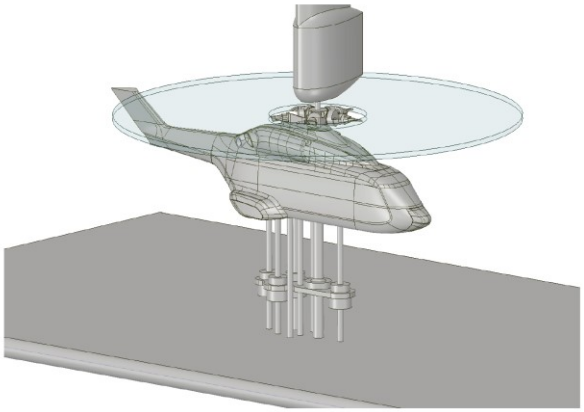

Figure 12: Visualization of the simulated helicopter geometry.

It is worth noting that the complete geometry of the rotor is not represented in the simulation. The additional computational cost associated with the representation of each of the rotor blades as well as the resolution of the flow generated by the rotation of the complete rotor would not be feasible within the framework of an industrial application. In order to minimize the computation time, it was therefore chosen to model the rotor downwash using an actuator disk. In this approach, the rotor is modeled through a virtual disk defined within the fluid volume at the rotor location (in light blue on Figure 12). Source terms are then added to the momentum transport equations inside this disk. These source terms are determined from the distribution of forces and moments on the rotor disk which are obtained from a preliminary calculation with the in-house code HOST. Rotor downwash is therefore modeled in the simulation by a jump in momentum applied to the fluid passing through the disk. The rotor head (whose geometry has been simplified) is, on the contrary, represented in order to take into account the blocking effect induced by its presence in the center of the actuator disc. However, it is worth noting that its rotation is not taken into account in the calculation.

Regarding the wind tunnel boundary conditions, a mass flow rate and a uniform static temperature field T_{cf} are prescribed at the domain inlet. Incoming mass flow value has been defined iteratively to get the correct velocity at the anemometer location. A static pressure condition equal to an atmospheric pressure of 1013.25 hPa is prescribed at the wind tunnel outlet. All the walls of the computational domain are considered adiabatic. From a dynamic point of view, slipping conditions have been assigned to the wind tunnel walls to avoid meshing the boundary layers in these areas and thus reduce the size of the mesh. The rest of the walls are however modeled with a no-slip condition.

The nozzle inlet boundary condition is prescribed upstream of the elbow located at the end of the vertical section of the pipe supplying the hot air to the nozzle. A detailed view of the location of the nozzle inlet is shown in Figure 13.

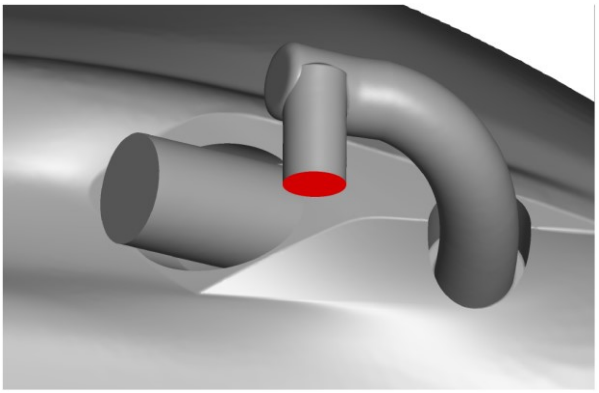

Figure 13: Sectional view of the interior of the fuselage showing the location of the jet inlet boundary condition (in red).

At the nozzle inlet, a mass flow rate corresponding to the measured flow rate as well as a uniform field of static temperature T_j are imposed. Regarding turbulent conditions, a level of turbulence T_u = 5% and a viscosity ratio v_t/v = 100.0 are imposed. Due to the presence of the elbow which is strongly disturbing the flow within the pipe, synthetic turbulence injection was not required at the nozzle inlet.

Finally, it should be noted that the gas ejected by the nozzle is composed exclusively of air in the simulation while it is in reality a mixture of burnt gases. In order to estimate the error made on the jet velocity at the nozzle outlet due to this assumption, it is considered that the mixture air-propane was injected into the combustion chamber in stoichiometric proportions (which is the case in practice). Therefore, complete combustion of propane can be assumed. The chemical reaction associated to the combustion of propane is given in Equation 1.

$$C_3H_8+5O_2 = 3CO_2 + 4H_2O \qquad (1)$$

Under this assumption and considering that the air is composed of 80% nitrogen (N_2) and 20% of oxygen (O_2) as a first approximation, it is possible to estimate the composition of the burnt gases ejected from the nozzle. For this, the following equation is used:

$$C_3H_8 + 5O_2 + 20N_2 = 3CO_2 + 4H_2O + 20N_2 \quad (2)$$

Presented at 48th European Rotorcraft Forum, Winterthur, Switzerland, 6-8 September, 2022

Under the temperature and pressure conditions at the ejection, one can compute the density of each of the species resulting from the combustion:

ρ_{CO2} (kg/m^{-3})	ρ_{N2} (kg/m^{-3})	ρ_{H2O} (kg/m^{-3})
0.581	0.370	0.238

Table 3: Densities of the chemical species constituting the burnt gases under the conditions of temperature and pressure at the nozzle outlet.

The equivalent density of the burnt gases is then computed by taking a weighted average of species densities where weights are the stoichiometric coefficients of the equation (2). The equivalent density for the mixture is then ρ_{burnt_gases} = 0.374 kg/m^3. This value is to be compared to the density of dry air ρ_{air} = 0.382 kg/m^3 under the same conditions of pressure and temperature. The mass flow rate at the ejection being known, it is then possible to compute the mean jet velocity at the nozzle outlet considering either burnt gases or air. Finally, the jet velocity at the nozzle outlet calculated under these two hypotheses only varies by 2%. This result allows us to justify the choice consisting in representing the exhaust gases by air only.

6.3. Mesh

The mesh used for the simulation of the helicopter configuration was generated using the software Fluent Meshing. The mesh is unstructured and composed of tetrahedral and prismatic elements. To ensure that cells are small enough in the jet region to solve the turbulent structures of the flow, a refinement box has been defined around the area of interest. A visualization of the location of this refinement box is presented in Figure 14.

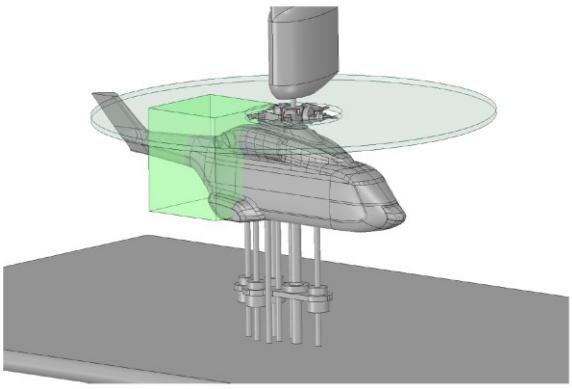

Figure 14: Visualization of the location of the mesh refinement area (in green) with respect to the helicopter model.

Within this refinement box (in green in Figure 14), the characteristic size of the mesh elements Δx is limited to a maximum value of 2 mm. Near the walls which are modeled with a no-slip condition, the mesh is refined in the normal direction using 12 layers of prisms. The height of the first cell is set to 10^{-4} m to get y^+ values lower than 5.0 over the entire fuselage and piping. The growth between two adjacent cells is governed by a geometric law whose ratio is fixed at 1.2. This allows for a gradual increase in the cell size and good resolution of the boundary layer. The final mesh consists of 91 million cells. Two visualizations of the mesh used are presented in Figure 15 and Figure 16.

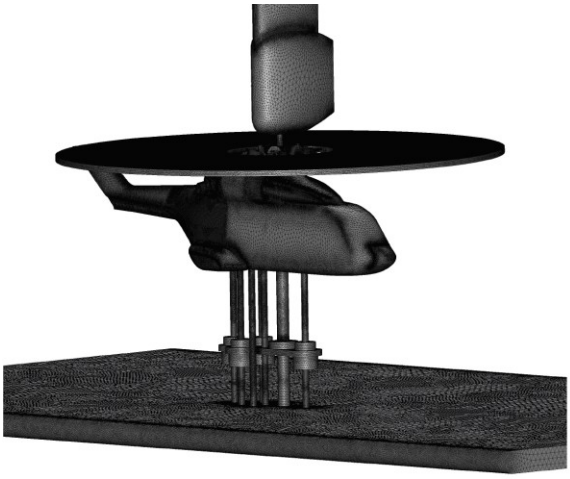

Figure 15: Visualization of the surface mesh over the helicopter.

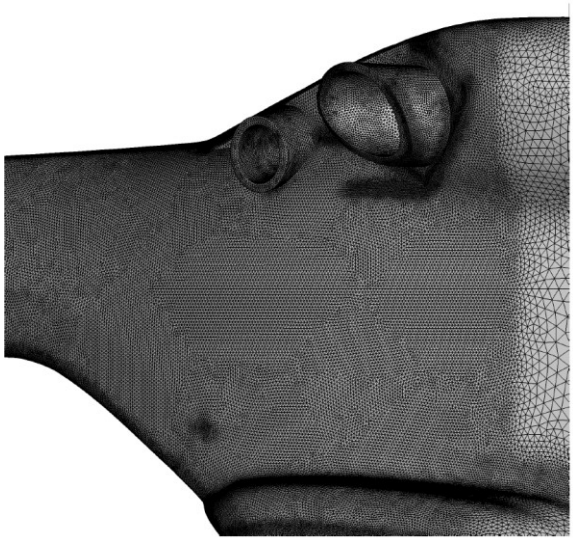

Figure 16: Visualization of the surface mesh near the nozzle outlet.

Presented at 48th European Rotorcraft Forum, Winterthur, Switzterland, 6-8 September, 2022

6.4. NUMERICAL SETTINGS

The simulation conducted on the helicopter configuration is carried out with the ANSYS Fluent software using the Scale-Adaptive Simulation approach coupled with a k−ω SST turbulence model as proposed by Menter & Egorov [87]. The numerical methods used for this simulation are similar to those of the calculations made on the simplified jet in crossflow configuration. As a reminder, they are defined in agreement with ANSYS best practices guidelines regarding scale-resolving simulations. Therefore, the Pressure-based solver was used. The pressure-velocity coupling is carried out using the SIMPLEC scheme [114]. A second-order upwind spatial discretization scheme is used to compute the convective fluxes of all transported quantities except momentum. For this simulation, the spatial discretization scheme Bounded Central Differencing (BCD) is used for the calculation of momentum convective fluxes. This choice is motivated by the instability of the central differencing scheme (CD), used for the simulations of the simplified jet in crossflow configuration, in the case of the helicopter simulation. For the simplified jet in crossflow configuration, the use of a numerical scheme that is less dissipative as the CD scheme had proved necessary due to the low level of initial instability of the flow. The numerical dissipation introduced by the BCD scheme did not make it possible to solve the large-scale turbulent structures in this specific case leading to a RANS-like solution. However, this behavior was not observed in the case of the helicopter simulation. The higher degree of instability of the flow at the ejection, due to the presence of the elbow in the blowing circuit, is likely to explain this difference in behavior between the two configurations. To finish, gradients are calculated using a least squares method. A second order implicit scheme is used for temporal discretization. A time step t = 1.10^{-5} s is used to obtain a convective CFL lower than 3.0 for all cells of the computational domain.

6.5. Results

Before starting the analysis of the results, it is worth checking the field of the turbulent to molecular viscosity ratio ν_t/ν in order to verify that the turbulence spectrum is mainly resolved in the jet region. As a reminder, the ratio ν_t/ν can be considered as an indicator of the way turbulence is handled by the model (modeled or resolved) in the case of hybrid approaches RANS/LES. The field of ν_t/ν in a plane perpendicular to the fuselage of the helicopter and passing through the center of the nozzle is shown in Figure 17.

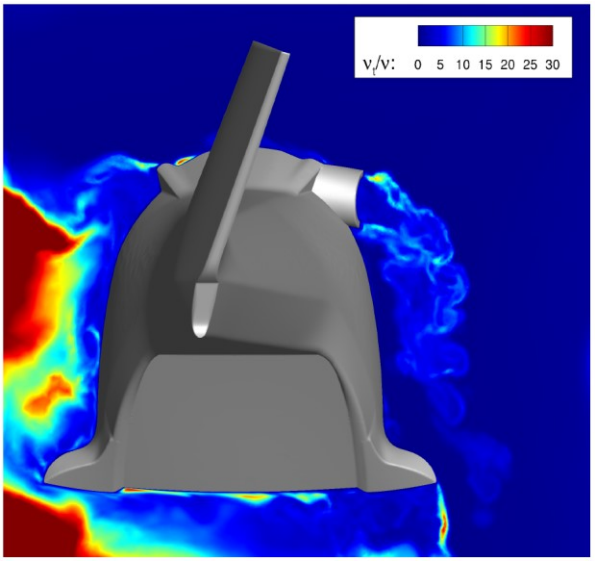

Figure 17: Field of ν_t/ν in a plane perpendicular to the fuselage of the helicopter and passing through the center of the nozzle (SAS-SST simulation).

In Figure 17, one can see that the levels of ν_t/ν are low in the jet region (typically less than 15 to 20). These are roughly of the same order as the levels observed for the simplified jet in crossflow configuration. Thus it can be assumed that the SAS-SST model is mainly working in its scale-resolving mode and that the turbulence of the flow is mainly resolved in the jet region. Moreover, this demonstrates that the destabilization of the flow caused by the presence of the elbow is sufficient to accelerate the RANS to LES transition of the model without resorting to synthetic turbulence injection at the nozzle inlet.

A visualization of the simulated jet is shown in Figure 18 using an instantaneous iso-surface of static temperature T = 60°C colored by the vertical component of the instantaneous velocity.

It can be seen that the jet produced by the nozzle is strongly deflected by the external flow composed of the rotor downwash, the wind tunnel flow and the ground effect. However, it can be emphasized that the deflection of the jet is mainly due to the rotor downwash. This observation can easily be verified by plotting the field of the vertical component of the mean velocity W in the center plane of the wind tunnel Y = 0 scaled by the wind tunnel speed V_s (Figure 19).

Presented at 48th European Rotorcraft Forum, Winterthur, Switzerland, 6-8 September, 2022

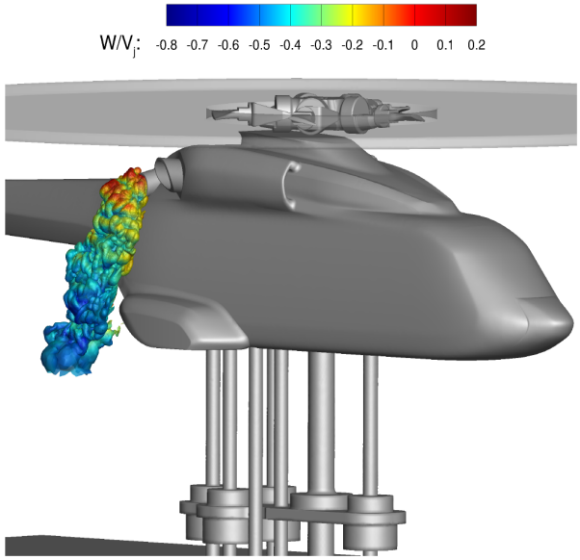

Figure 18: Visualization of the jet using an instantaneous static temperature iso-surface T = 60°C colored by the vertical component of the instantaneous velocity normalized by the mean jet velocity at the nozzle outlet V_j (SAS-SST simulation).

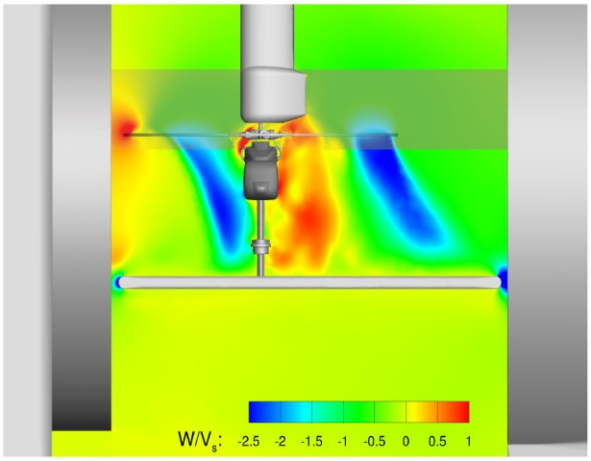

Figure 19: Field of the vertical component of the mean velocity W in the center plane of the wind tunnel Y = 0 scaled by the wind tunnel speed V_s (SAS-SST simulation)

Figure 19 reveals that the velocities induced by the rotor are about twice that of the wind tunnel flow. Therefore, rotor downwash modeling is a first-order parameter to get the correct prediction of the jet deflection. It is also noted that the wind tunnel flow strongly influences the topology of the velocity field induced by the presence of the rotor. This rotor notably induces a deviation of the rotor flux downstream. In conclusion, it should be noted that the interaction of the wind tunnel flow with the rotor downwash is complex and that its good restitution by simulation is critical in order to correctly predict the trajectory of the jet.

In order to compare the simulated and measured temperature levels close to the fuselage, virtual probes were placed in the simulation. The positioning of these probes corresponds to the locations of the thermocouples used during the wind tunnel tests as shown in Figure 20.

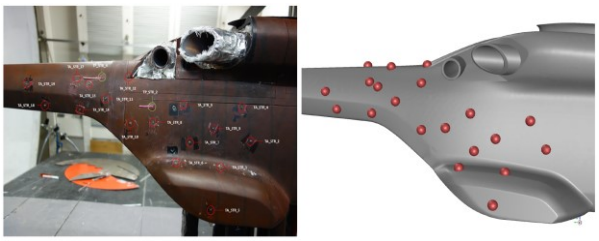

Figure 20: Comparison of the positioning of the thermocouples during the wind tunnel tests with the positioning of virtual probes in the CFD calculation.

These virtual probes are represented by spheres in Figure 20 to ease their visualization. These virtual probes are used to extract the mean static temperature values from the simulation at the location of each of the thermocouples. The temperatures obtained by simulation are then compared to the thermocouple measurements. An interpolation, on the fuselage of the helicopter, of the normalized mean static temperatures θ measured by the thermocouples and obtained at the location of the virtual probes placed in the SAS-SST simulation is shown in Figure 21

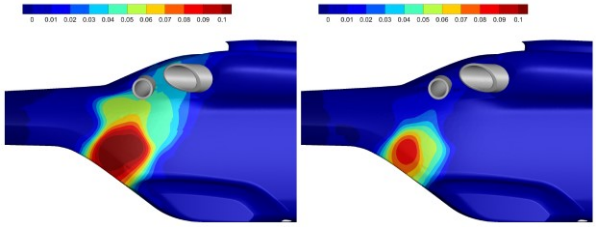

Figure 21: Interpolation of the normalized mean static temperatures θ on the helicopter fuselage measured by the thermocouples (left) and by the virtual probes placed in the SAS-SST simulation (right).

The interpolation method used to map the temperature fields is based on inverse distance weighting. It is to be emphasized that this approach does not provide an accurate visualization of the jet thermal footprint on the fuselage. Nevertheless, it allows to qualitatively and visually compare the data from experiments and simulation. The plots in Figure 21 reveal that both the temperature levels as well as the extent of the thermal footprint are underestimated in the simulation. However, it is worth highlighting that the localization of the hot spot is well captured by the simulation. Given the uncertainty on the thermocouples positioning

Presented at 48th European Rotorcraft Forum, Winterthur, Switzerland, 6-8 September, 2022

during tests (no precise coordinates available), a sensitivity study was conducted on the position of the virtual probes, representing the thermocouples in the simulation, by creating a sphere around each of them and collecting the maximum and minimum temperature values at the surface of these spheres. The radius of the sphere is set to 4 mm. This analysis revealed large differences between the temperature at the probe and the minimum and maximum temperatures at the surface of the sphere. This finding is however not surprising due to the strong temperature gradients observed within the jet. It must be noted that the greatest temperature variation is obtained when moving the probe in the direction normal to the wall. Thus the maximum temperature at the surface of the sphere is obtained by a displacement of 4mm of the virtual probe in the direction normal to the wall while moving away from it. An interpolation, on the fuselage of the helicopter, of the normalized mean static temperatures measured by the thermocouples and by the virtual probes shifted by 4mm away from the wall with respect to their estimated position is shown in Figure 22.

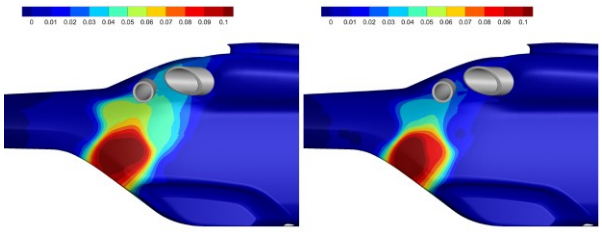

Figure 22: Interpolation of the normalized mean static temperatures θ on the helicopter fuselage measured by the thermocouples (left) and by the virtual probes shifted 4mm awat from the wall in the SAS-SST simulation (right).

It can be noticed that the thermal footprint of the jet is in better agreement with the experimental measurements. The extent, location and intensity of the jet thermal footprint are correctly reproduced event though simulated temperatures are slightly lower than those measured at the probes "TA_STR9" and "TA_STR12" (see Figure 20). The fact that a correct thermal footprint is recovered when moving the virtual probes an additional 4mm away from the fuselage may have several explanations. This distance being very small, it may be due to a slight underestimation of the rotor induced velocities due to its modeling resulting therefore in a lower deflection of the jet. On the other hand, the measurement uncertainty on the mass flow rate at the nozzle outlet is estimated to be about +/-3%. Although this is low, a slightly lower mass flow rate in the tests compared to the one specified in the simulation could explain the observed differences. These hypotheses could not be verified within the framework of this study due to time constraints but constitutes one of the ways forward regarding the work presented in this paper.

7. CONCLUSIONS

The present work investigates the capability of aerothermal CFD simulations to correctly reproduce trajectory and mixing of engine exhaust gases in order to support design. Different Steady RANS and SAS/LES approaches were first compared on a dedicated hot jet in crossflow database collected at ONERA. . It was shown that even advanced RANS modelling could not reproduce the jet mixing with a high level accuracy, contrary to unsteady methods.

A SAS-SST simulation was then conducted on an industrial configuration based on a helicopter mock-up was presented. The objective was to demonstrate the applicability of the approach SAS-SST in an industrial context. For this, a simulation was carried out at a test point from an experimental database generated during a test campaign conducted in Marignane wind tunnel Airbus Helicopters. During this test campaign, a mock-up equipped of a 5-blade rotor with twisting law was used. The mock-up also has a circuit of hot air blowing to simulate the ejection of engine exhaust. Nearby temperatures of the helicopter's fuselage were measured using thermocouples installed on the mock-up to characterize the thermal trace of the hot gases. The study was limited at a test point for which only one nozzle is in operation. The results obtained first highlighted that rotor blast modeling is a first-order element for the good prediction of jet deflection. In addition, good restitution of interaction of the wind tunnel flow with the rotor downwash is also decisive in order to correctly predict the trajectory of the jet. From a thermal point of view, it was found that the temperature levels measured by the thermocouples were well rendered by simulation at a slightly greater fuselage distance (in the order of a few millimeters). Two parameters could explain this observation, the modelling of the rotor downwash and the value of the mass flow prescribed at nozzle outlet. Since these assumptions could not be verified, the question remains open and will drive future works on this subject.

8. ACKNOWLEDGMENTS

The authors acknowledge the financial support of French Direction Generale de l'Aviation Civile in the framework of the CHARME research program.

Presented at 48th European Rotorcraft Forum, Winterthur, Switzterland, 6-8 September, 2022

9. REFERENCES

[1] Margason, R.J., 1993. Fifty years of jet in cross flow research. In: AGARD-CP-534, Computational and Experimental Assessment of Jets in Cross Flow, 1–1 to 1–41.

[2] Mahesh, K., 2013. The interaction of jets with crossflow. Annu. Rev. Fluid Mech. 45, 379–407.

[3] Karagozian, A.R., 2014. The jet in crossflow. Phys. Fluids 26 (10), 1–47.

[4] Sutton, O.G., 1932. A theory of eddy diffusion in the atmosphere. Proc. R. Soc. London Ser. A 135 (826), 143–165.

[5] Bosanquet, C., Pearson, J., 1936.The spread of smoke and gases from chimneys. Trans. Faraday Soc. 32, 1249–1263.

[6] Gentry, G., Jr, Margason, R., 1968. Aerodynamic characteristics of a five jet VTOL configuration in the transition speed range. Technical Note NASA TN D-4812, NASA.

[7] Hale, C., Plesniak, M.W., Ramadhyani, S., 2000. Film cooling effectiveness for short film cooling holes fed by a narrow plenum. J. Turbomach. 122 (3), 553–557.

[8] Ivanova, E., Di Domenico, M., Noll, B., Aigner, M., 2009. Unsteady simulations of flow field and scalar mixing in transverse jets. In: ASME Turbo Expo 2009: Power for Land, Sea, and Air. American Society of Mechanical Engineers, pp. 101–110.

[9] Bézard, H., Donjat, D., Viguier, P., Jouhaud, J.C., Bocquet, S., 2012. Projet ASTHER – Analyse et Simulation des jets d´ebouchants et de leur impact THERmique, Technical Note 2/15118 DMAE, ONERA.

[10] Galeazzo, F.C.C., Donnert, G., C´ardenas, C., Sedlmaier, J., Habisreuther, P., Zarzalis, N., Beck, C., Krebs, W., 2013. Computational modeling of turbulent mixing in a jet in crossflow. Int. J. Heat Fluid Flow 41, 55–65.

[11] Prause, J., Emmi, Y., Noll, B., Aigner, M., 2016. LES/RANS Modeling of Turbulent Mixing in a Jet in Crossflow at Low Velocity Ratios. In: 54th AIAA Aerospace Sciences Meeting, 0609.

[12] Rusch, D., Blum, L., Moser, A., R¨osgen, T., 2008. Turbulence validation for fire simulation by CFD and experimental investigation of a hot jet in crossflow. Fire Saf. J. 43 (6), 429–441.

[13] Yuan, L.L., Street, R.L., Ferziger, J.H., 1999. Large-eddy simulations of a round jet in crossflow. J. Fluid Mech. 379, 71–104.

[14] Kamotani, Y., Greber, I., 1972. Experiments on a turbulent jet in a cross flow. AIAA J. 10 (11), 1425–1429.

[15] Harms, L., “Experimental investigation of the flow field of a hot turbulent jet with lateral flow,” NASA TT F 15, 707, Vol. Part I, 1974.

[16] Paysant, R., Laroche, E., Millan, P. and Buet, P., "RANS Modelling of a High-Temperature Jet in a Cold Crossflow: from Eddy Viscosity Models to Advanced Anisotropic Approaches," AIAA 2021-1542. AIAA Scitech 2021 Forum. January 2021

[17] Jarrin, N., Prosser, R., Uribe, JC, Benhamadouche, S., Laurence, D., Reconstruction of turbulent fluctuations for hybrid RANS/LES simulations using a Synthetic-Eddy Method, International Journal of Heat and Fluid Flow 30 (2009) 435{442.

[18] M. L. Shur, P. R. Spalart, M. K. Strelets, A. K. Travin, Synthetic turbulence generators for RANS-LES interfaces in zonal simulations of aerodynamic and aeroacoustic problems, Flow, turbulence and combustion 93 (2014), 63-92.

[19] Paysant, R., Laroche, E., Troyes, J., Donjat, D., Millan, Buet, P., Scale resolving simulations of a high-temperature turbulent jet in a cold crossflow: Comparison of two approaches, International Journal of Heat and Fluid Flow,Volume 92,2021,108862, https://doi.org/10.1016/j.ijheatfluidflow.2021.108862

[20] Guillet, F. Essais soufflerie. Tech. rep., Airbus Helicopters, Marignane.

Presented at 48th European Rotorcraft Forum, Winterthur, Switzerland, 6-8 September, 2022